EurJIC
European Journal of Inorganic Chemistry

Full Papers
doi.org/10.1002/ejic.202100137

Chemistry Europe
European Chemical Societies Publishing

Structure Effects Induced by High Mechanical Compaction of STAM-17-OEt MOF Powders

Angela Terracina,[a, b] Lauren N. McHugh,[c] Matjaz Mazaj,[d] Nika Vrtovec,[d, e] Simonpietro Agnello,[a] Marco Cannas,[a] Franco M. Gelardi,[a] Russell E. Morris,[c] and Gianpiero Buscarino*[a]

Metal-organic frameworks (MOFs) are promising materials for many potential applications, spacing from gas storage to catalysis. However, the powder form they are generally made of is not suitable, mainly because of the low packing density. Powder compaction is therefore necessary, but also challenging because of its typical mechanical fragility. Indeed, generally, MOF powders undergo irreversibly damages upon densification processes, for example partially or totally loosing microporosity and catalytic activity. In this work, we have deeply studied the compaction effects on the flexible Cu(II)-based MOF STAM-17-OEt ($Cu(C_{10}O_5H_8)\cdot 1.6\ H_2O$), whose chemical composition is close to that of HKUST-1, obtaining that, by contrast, STAM-17-OEt is extremely suitable for mechanical compaction processes with pressures up to 200 MPa, which increase its packing density and its catalytic activity, and then also preserve the characteristic porosity, flexibility and water stability of STAM-17-OEt. The results are supported by many experimental techniques including EPR spectroscopy, PXRD diffraction, CO_2 isotherms studies and catalytic tests.

Introduction

Metal–organic frameworks (MOFs) are a class of microporous crystalline materials, suitable for several potential applications.[1] Furthermore, the so-called third generation of MOFs characterized by the flexible MOFs, combining the crystallinity of the lattice with a cooperative structural transformability,[2] got a strong attention of the scientific community because of their further potentialities. Unfortunately, however, only an extremely small percentage of MOFs is flexible. In addition, there are two important obstacles to overcome before the employ of different MOFs in a systematic industrial-scale development: the typical limited chemical stability with respect to water and their large-scale synthesis in powder form.[3–6] Surprisingly, the new MOF STAM-17-OEt ($Cu(C_{10}O_5H_8)\cdot 1.6\ H_2O$) combines all these extraordinary properties: it is flexible (or better, hemilabile),[7–9] extremely water-stable,[7,8,10] and with this work we show that it is also very resistant to the mechanical pressures necessary for the industrialization of the material, and therefore easy to densify and commercialize even if originally synthesized in powder form. This last aspect is not at all trivial, because in literature many MOFs have been subjected to densification processes with or without the help of chemical binders, but in most cases a significant loss of crystallinity and surface area have been found, compromising the typical performances of the material, especially as adsorbent or catalyst.[4,11–21] Recently, after many unsuccessful attempts,[4,11–13] it has been found that HKUST-1 (or Cu-BTC), which is considered a reference system for all of the copper paddle wheel MOFs like STAM-17-OEt, is actually very easy to compact if the appropriate protocol is applied.[22] However, HKUST-1 is very sensitive to water and it typically undergoes severe hydrolysis even by limited exposure to air.[8,22–25] In this work, we have tested the effectiveness of a similar compaction protocol to the water-proof and hemilabile STAM-17-OEt. This latter Cu-based MOF, like HKUST-1, is formed by a paddle-wheel unit structure composed of two copper ions coordinated by four carboxylate bridges.[7,8,26] Such carboxylate groups arise from 5-ethoxy isophthalate organic linkers.[7,8] The lattice of this MOF is composed by an infinite 2D framework with kagome-type topology. Similarly to HKUST-1, a crystallization water molecule occupies the apical coordination site on each of the Cu^{2+} ions of the paddle-wheels, establishing hydrogen bonds to the coordinated carboxylate oxygen atoms lying on the 2D sheets above and below.[7] Its particular hemilability arises right from the removal (or addition, during hydration processes) of such coordinated water molecules,

[a] Dr. A. Terracina, Prof. S. Agnello, Prof. M. Cannas, Prof. F. M. Gelardi, Prof. G. Buscarino
Dipartimento di Fisica e Chimica - Emilio Segrè,
Università di Palermo,
Palermo 90123, Italy
E-mail: gianpiero.buscarino@unipa.it
[b] Dr. A. Terracina
Dipartimento di Fisica e Astronomia,
Università di Catania,
Palermo 95123, Italy
[c] Dr. L. N. McHugh, Prof. R. E. Morris
EaStCHEM School of Chemistry,
University of St Andrews,
Purdie Building, St Andrews, United Kingdom
[d] Dr. M. Mazaj, Dr. N. Vrtovec
National Institute of Chemistry,
Hajdrihova 19, Ljubljana 1000, Slovenia
[e] Dr. N. Vrtovec
Faculty of Inorganic Chemistry and Technology,
University of Ljubljana,
Večna po 113, 1000 Ljubljana, Slovenia

Supporting information for this article is available on the WWW under https://doi.org/10.1002/ejic.202100137

process that leads to a single-crystal to single-crystal transition.[7–9] The two Cu^{2+} ions involved in the paddle-wheels confer to STAM-17-OEt (as well as to HKUST-1) peculiar magnetic properties: the two S = 1/2 spins establish an antiferromagnetic coupling characterized by a spin angular momentum with a singlet (S = 0) ground state and a triplet (S = 1) excited state.[22,23,27–30] The latter state generates a characteristic Electron Paramagnetic Resonance (EPR) spectrum.[8,10] Regarding STAM-17-OEt, these peculiar magnetic properties have been successfully used in previous works to study the hemilability and the other effects induced by hydration in this material,[8] as well as in composite systems involving active carbon,[10] by analyzing the changes in the EPR spectrum. More in detail, in a previous study concerning the hydration effects on STAM-17-OEt, we observed that the crystal transitions induced by both the processes of hydration and dehydration have remarkable magnetic consequences. These effects can thus be used to understand the particular lattice configuration of STAM-17-OEt in any condition by the acquisition of an EPR spectrum.[8] Furthermore, such magnetic properties may also potentially give information about the degree of damages induced by the mechanical compaction.[22] In fact, in a previous work concerning HKUST-1, the effects of the densification induced by mechanical pressure have been successfully studied by EPR spectroscopy, which has allowed to estimate the percentage of paddle-wheels damaged by the pressure.[22] Such estimation has been possible through the study of the changes in intensity of a specific EPR resonance, peaked at about 350 mT and with a peak-to-peak width of about 40 mT.[22] More in detail, in this spectral region we can observe the EPR signal of paramagnetic Cu^{2+} ions with electron spin S = 1/2. In the pristine HKUST-1 or STAM-17-OEt material these centers arise from extra-framework complexes involving a copper ion coordinated with six water molecules, $[Cu(OH_2)_6]^{2+}$, that are just synthesis defects.[8,22,23,27] In addition, it has been previously shown for HKUST-1 that, when the network is distorted or damaged by mechanical compaction or by exposure to air moisture, other different contributions may also appear in the same spectral region, with features very similar to those assigned to the $[Cu(OH_2)_6]^{2+}$ complexes.[8,22,23] These additional signals are also due to the spin 1/2 of the Cu^{2+} ions, but in this case they arise from decoupled copper paddle-wheels, which have lost the antiferromagnetic coupling because of the pressure or the interaction with water.[8,22,23] Consequently, it is possible to obtain a quantitative estimate of the damages induced by a specific treatment on MOFs involving copper paddle-wheels by just monitoring the changes induced in the intensity of the resonance centered at about 350 mT.[22] In the present paper, we have investigated the effects induced by mechanical compaction on the structure and on the flexibility (hemilability) of STAM-17-OEt by EPR, Raman and FTIR spectroscopies, powder X-ray diffraction (PXRD), nitrogen and carbon dioxide isotherms, optical and atomic force microscopies (AFM). We also tested the catalytic activity of STAM-17-OEt as pristine powder and as densified tablet.

Results and Discussion

Figure 1 shows the spectra of a sample of powder of activated STAM-17-OEt (black line) and of hydrated STAM-17-OEt (purple line) acquired at 77 (a) and 300 K (b).

The spectra show the typical resonances of STAM-17-OEt.[8,10] The three peaks centered at about 15, 470 and 600 mT observed at 77 K arise from triplet (S = 1) state.[8,10,22,23,27–30] The EPR signal centered at about 350 mT in the STAM-17-OEt spectra (Figure 1(a)) arises from the copper-based complexes $[Cu(OH_2)_6]^{2+}$.[8,22,23,27] The intensity of this latter EPR signal (peaked at about 350 mT) vary slightly from one sample to another, depending on the amount of such synthesis defects.[8] The EPR spectrum acquired at 300 K of STAM-17-OEt consists of a large symmetric curve centered at about 350 mT which arises from the triplet centers.[8] The intensity of the signal is very sensitive to the hydration degree of the material.[8] Peaks similar to those above described are easily detectable also in the EPR spectra acquired for HKUST-1, due to the involvement of similar paddle-wheels structures.[8,22,23,27,28,30] The EPR signals obtained for activated and hydrated STAM-17-OEt differ significantly in many aspects at both temperatures, and some of such differ-

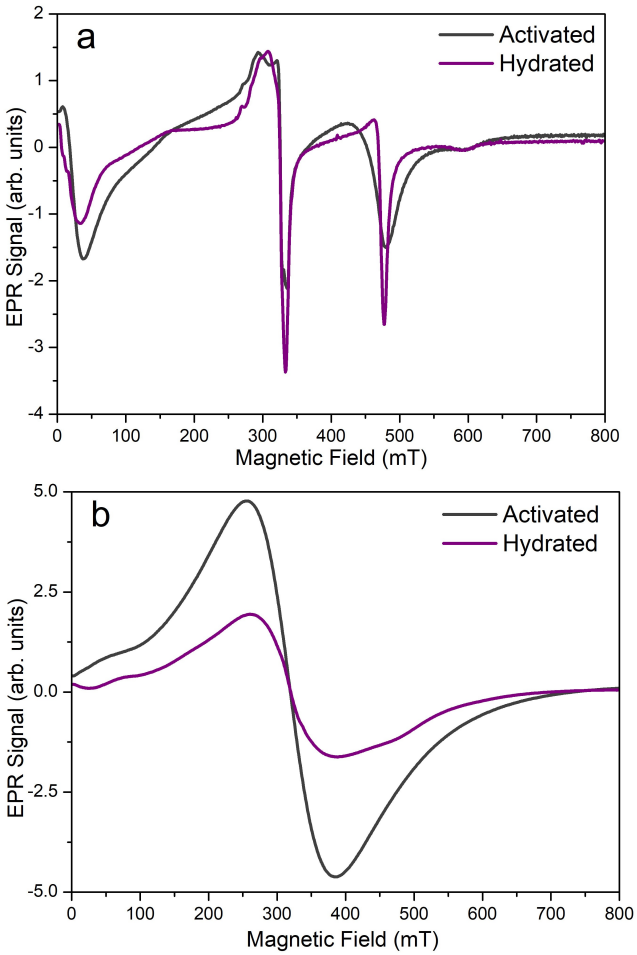

Figure 1. EPR spectra obtained at 77 (a) and 300 K (b) for a sample of STAM-17-OEt powder activated (black) and hydrated (purple).

ences are directly related to the hemilability of the material.[8] First of all, at 77 K, in the hydrated spectra the peak at 470 mT is significantly narrower and with a larger amplitude than the equivalent features in the spectrum of the activated powder. Such variations in lineshape are due to the flexibility of the material:[8] the inter paddle-wheel connections change when, as a consequence of the adsorption of water molecules, the crystal transition occurs, leading the framework to a structural arrangement with a higher order.[7,8] The increase of the crystalline order determines the reduction of the inhomogeneous component of the EPR line width.[8] Furthermore the peak at about 15 mT shows a progressive shift to lower fields, accompanied by the appearance of a fine structure.[8] The differences between the lineshapes of the two spectra acquired at 300 K are less marked but small shoulders are visible in the hydrated samples both at low fields and at about 460–490 mT; the stronger difference between the two spectra is the intensity,significantly higher in the activated sample than in the hydrated one.[8] This latter aspect seems to be characteristic of the copper paddle-wheel unit based MOFs; in fact, it has been also observed in HKUST-1 after few hours of exposure to air moisture.[8,22,23] It is also known that for STAM-17-OEt material the transitions between the hydrated and activated configurations are totally reversible in the powder material but it is unknown if this property is preserved in the mechanically compacted samples.[7,8] In order to study the effects of mechanical compaction on powder of STAM-17-OE, we have prepared tablets starting from activated powders using different pressures ("set A"), following the optimized protocol defined in our previous work[22] for HKUST-1. The prepared samples have been measured by EPR, re-hydrated and measured again to evaluate the reversibility of the hydration process in the compacted samples (see Experimental section for more details). In addition, a second set of tablets ("set B") has been obtained starting from hydrated powders, for comparison. The EPR spectra obtained at 77 K for the tablet set A are shown in Figure 2: STAM-17-OEt in powder form before any mechanical treatment (a) and after the compaction (and the reactivation) at a pressure equal to 3 MPa (b), 20 MPa (c), 50 MPa (d), 100 MPa (e) and 200 MPa (f). In Figure 3 the correspondent EPR spectra acquired at 300 K are shown.

The spectra of Figure 3 show virtually indistinguishable features, whereas the spectra in Figure 2 show just small differences arising only from the peak at about 350 mT. However these discrepancies are not significant, because they do not show any systematic dependence on the pressure applied during the compaction of the powders and also because the amplitude of the peak in each spectrum is lower or at most comparable with that observed in the spectrum of the pristine powder. These differences are quantitatively comparable with the variability of the amount of pre-existing defects observed in the pristine powders and consequently they are naturally attributed to it. The reason why the spectra in Figure 3 do not show any difference lies in the origin of the large curve obtained at room temperature. In fact, these spectra are characterized by an EPR signal arising mostly from the triplet centers mainly because of the large susceptibility (Bleaney-Bowers's law) of these centers at high temperatures. This lack of resolution for $S = 1/2$ spin centers is also the reason why in the following we will essentially focus on the EPR spectra acquired at 77 K, like it has been done in previous work concerning HKUST-1 tablets.[22]

Figure 4 shows the EPR spectra obtained at 77 K for some representative re-hydrated tablets (set A). The correspondent spectra acquired at 300 K are included in Figure S1 (see Supporting Information). As shown, each spectrum exhibits the typical spectroscopic features of the EPR spectra obtained for hydrated STAM-17-OEt (compare with Figure 1). The presence

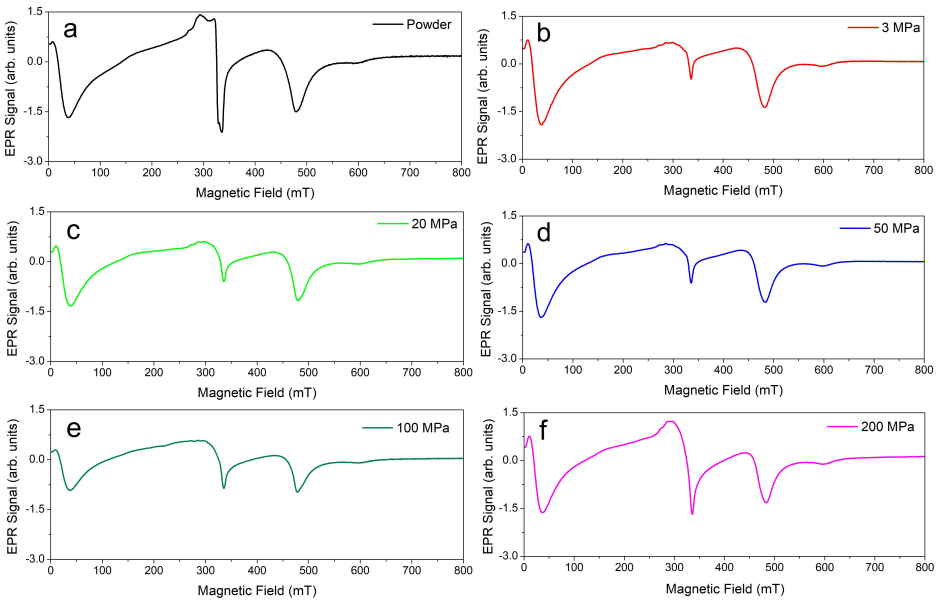

Figure 2. EPR spectra of the most significant tablets (set A) acquired at 77 K.

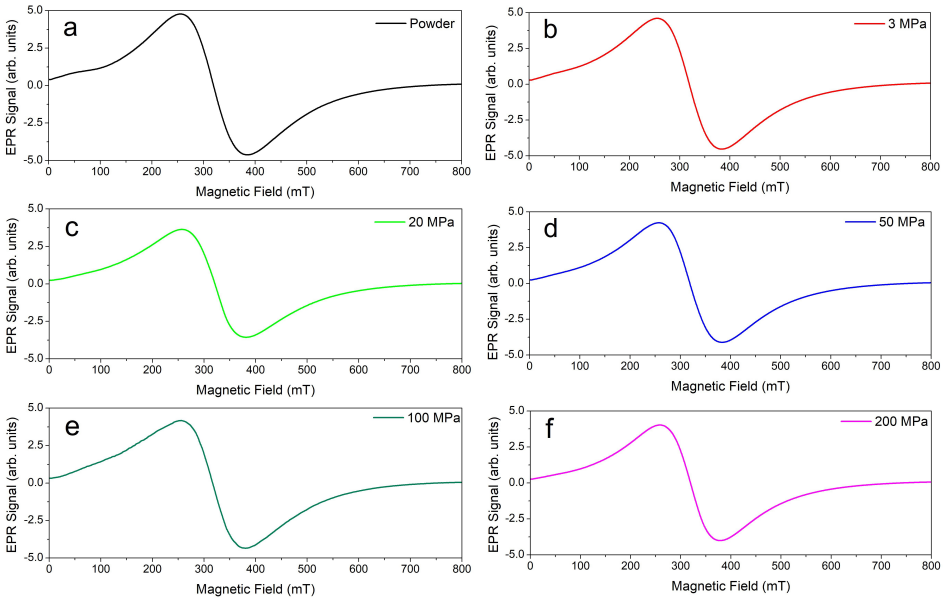

Figure 3. EPR spectra of the most significant tablets (set A) acquired at 300 K.

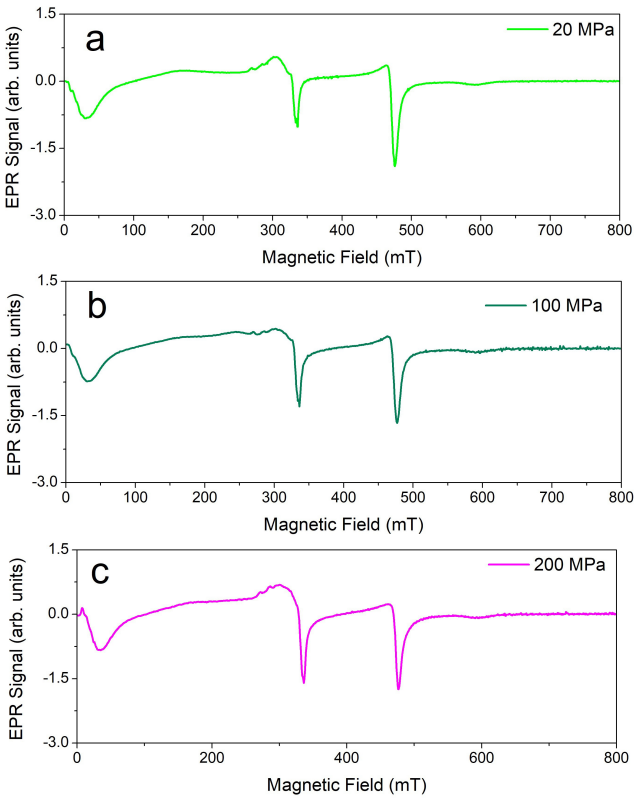

Figure 4. EPR spectra of the most significant tablets acquired at 77 K after the re-hydration.

of these features proves that reversible flexibility of the material is preserved. Furthermore, the absence of any sign of decomposition in the EPR spectra in Figure 4 and S1, indicates that the tablets of STAM-17-OEt have also preserved the strong stability towards exposure to water, a characteristic of the pristine powders. In other words, the outstanding stability of STAM-17-OEt is not affected by the mechanical compaction up to at least 200 MPa.

In order to further support this conclusion, X-ray diffraction measurements have been performed. Figure 5 shows the PXRD patterns acquired for the most significant samples of the set A. The tablets used (and the powder sample measured for comparison) have been re-hydrated, because each PXRD measurement requires many hours during which the sample is left in air and consequently it is not possible to catch the pattern of the activated samples. The diffraction pattern of the powder sample (Figure 5, black line) shows the well-known characteristic peaks of this material in hydrated form.[7,8] The PXRD patterns of the tablets are virtually indistinguishable compared to that of the powder sample, with peaks of comparable intensity and position, with the exception oftwo new small peaks at 11.5° and 12° in the patterns pertaining to the tablets samples, indicating that minor but detectable distortions of the long range structure of the material are actually induced.

Figure 6 shows the EPR spectra at 77 and 300 K acquired for a tablet of STAM-17-OEt of the set B produced with a pressure of 100 MPa, measured after each step in chronolgical order: activated powder form (a–b), hydrated powder (c–d), pressed at 100 MPa (e–f), after reactivation (g–h) and after the re-hydration (i–j). In each of these measurements we easily recognize the characteristic features of the activated material (6 (a),(b),(g),(h)) or of the hydrated one (6 (c),(d),(e),(f),(i),(j)). The correspondent spectra of the tablet 50 MPa and 200 MPa of the set B are shown in Figure S2 and S3, respectively (see Supporting Information). All these results confirm that the flexibility is preserved in STAM-17-OEt material even when it is pressed

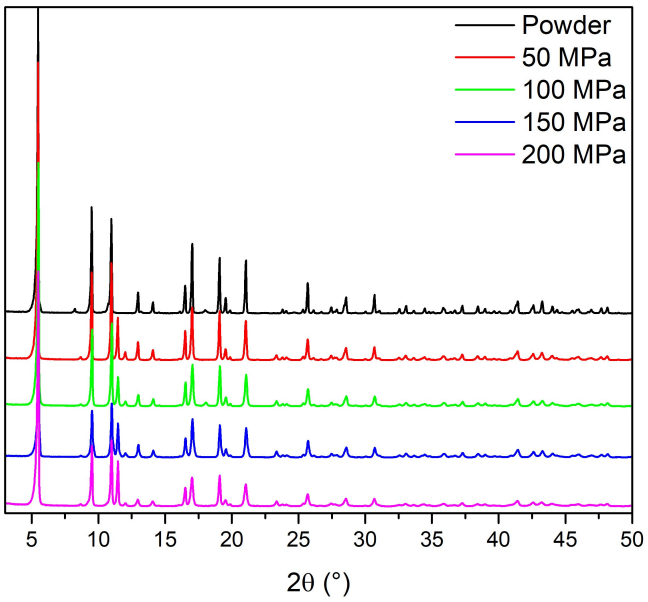

Figure 5. PXRD patterns acquired for powder and for the tablets pressed at 50, 100, 150, 200 MPa.

starting from hydrated powders. This result is very important because it has been seen for HKUST-1 that a very small degree of hydration is sufficient to irreversibly damage the material upon compaction. At variance, the EPR data reported here (Figure 6, S2 and S3) clearly show that there are neither signs of degradation of the material nor impacts on its flexibility. Both these results reasonably arise from the stronger resistance to water of STAM-17-OEt compared to HKUST-1.

A further deep characterization of the compacted powders of STAM 17-OEt has been performed by vibrational spectroscopies. Figure S4 shows the Raman spectra acquired for a set of representative tablets of the set A. The Raman spectrum of STAM-17-OEt in powder form shows its characteristic peaks.[8] The doublet at 200–221 cm^{-1} are assigned to vibrational modes involving the Cu^{2+} couple, whereas the peak at 276 cm^{-1} arises from an out-of-plane stretching of the Cu–O_{water}, where O_{water} is the oxygen of the water molecule linked to the Cu^{2+} ion.[8] Similarly, the peak at 496 cm^{-1} can be attributed to the stretching modes of the bond Cu–O involving a carboxylate oxygen and the copper ion.[8] At higher wavenumbers we can find vibrational modes attributed to bonds involving the organic linker, in particular at 747, 807, 1006, 1326, 1519 and 1606 cm^{-1}.[8] In addition, the peaks at 1394, 1425 and 1456 pertain to the symmetric and asymmetric stretching modes of the COO groups.[8] Figure S4 shows that no significant changes are recognizable between the spectra of the powder and those of the tablets, neither in the peaks directly involving the paddle-wheels, nor in those pertaining the organic part. This result gives a further strong support to the conclusion that the compaction process does not affect significantly the short/intermediate range structure of STAM-17-OEt.

The same conclusions have been obtained by the analysis of FTIR spectra. The FTIR measurements have been performed on different (set A) tablet samples and on the powder STAM-17-OEt for comparison. The results are shown in Figure S5. The spectra obtained are remarkably similar, displaying the same peaks and without any meaningful difference of the relative intensities between the peaks. In Figure 7 the spectra acquired for the powder and for the tablet obtained with a pressure of 200 MPa are superimposed: it can be easily observed that they are indeed virtually indistinguishable.

The values of measured and calculated densities of the samples considered in the present work are shown in Table S1 and S2, respectively. The calculated densities for a grain of pristine powder of STAM-17-OEt are 1.479 for the as made (hydrated) material[7] and 1.652 for the activated one.[7] The density estimated for the sample compacted with a pressure of 200 MPa (in its activated form) is ~1.6 g/cm^3, a value very close to that calculated for the ideal crystalline bulk structure. A picture of the sample just pressed with a pressure of 200 MPa is shown in Figure S6, whereas Figure S7 shows pictures of the tablets of set B.

Figure S8 and S9 show some optical images acquired for the powder sample and the 100 MPa (set B) respectively. On the basis of Figure S8 we have recognized that the powdered sample consists of single grains of variable sizes, ranging from a few to some tens of micrometers. In Figure S9 the compaction of the grains is well evident, but the granular form of the material is virtually unaltered. Studying the same samples with atomic force microscopy (AFM), we obtained the images reported in Figure S10 and S11. The two samples do not show any significant difference in the morphology : in both the couples of images we can recognize wide smooth surfaces in correspondence of the larger grains and rough areas associated to the presence of large aggregates of smaller grains.

Figure S12 shows the obtained N_2 isotherms for the powder sample and the tablets. The isotherm curve acquired for the powder sample is comparable to those previously reported in literature[8,10] and the same applies for the BET surface area calculated, which is about 61 m^2/g (see Table S3). The curve indicates a nearly type I shape, suggesting a microporous structure. At relative pressures $p/p_o > 0.85$ there is a slight increase of the N_2 uptake, indicating interparticle porosity that is most probably due to an agglomeration of individual crystallites. The tableting apparently has an effect on microporosity of the STAM-17-OEt material: an initial decreasing of the BET surface area has been calculated when a pressure of 20 MPa has been applied to the MOF, whereas only small differences are detected when the pressure is further increased. On the other hand, the curves also show an increase of the total pore volume: this is most probably a consequence of the mesoporous void generation between particles during the compression, and it becomes more and more prominent with the applied pressure. However, it is of fundamental significance to point out that STAM-17-OEt is a flexible structure, that is it undergoes structural transformation upon activation/dehydration processes or more in general upon interaction with specific guest molecules. For this reason, in cases like this, BET specific surface areas are not straightforwardly correlated with the sorption behavior of the material involved.[2,31] Moreover, the

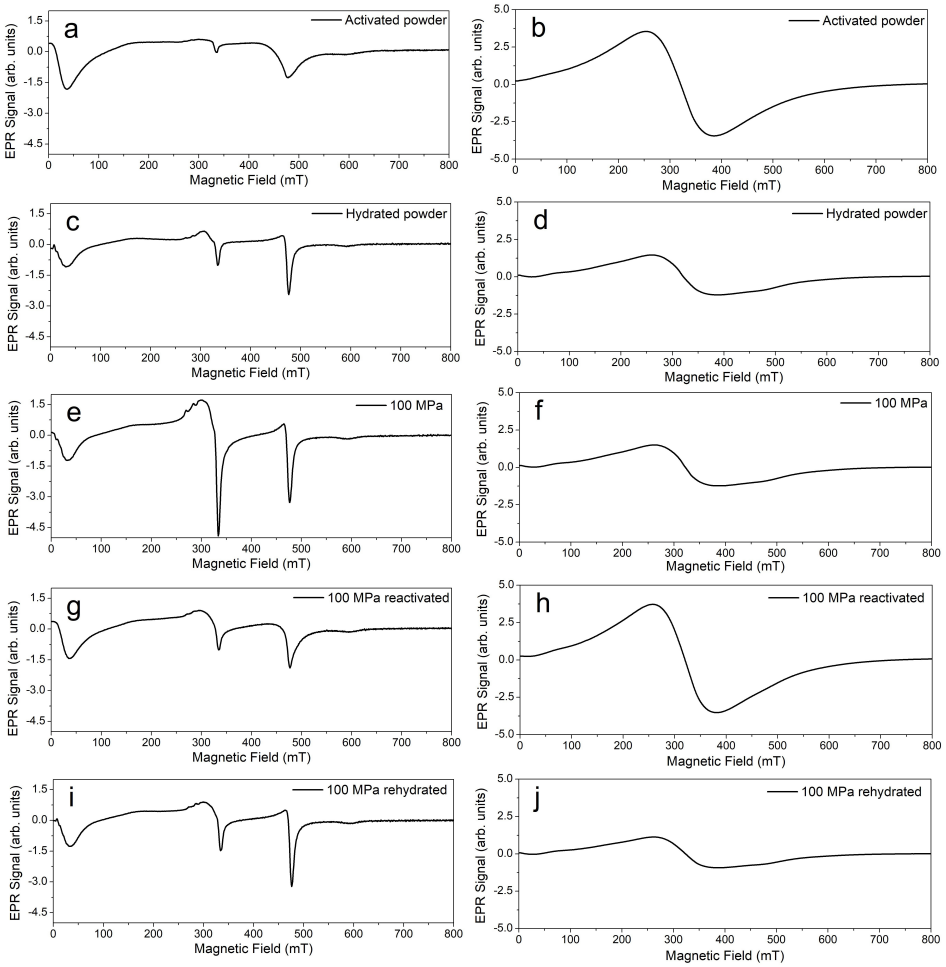

Figure 6. EPR spectra obtained at 77 (a-c-e-g-i) and 300 K (b-d-f-h-j) during the different steps of production of the 100 MPa tablet produced from hydrated powders.

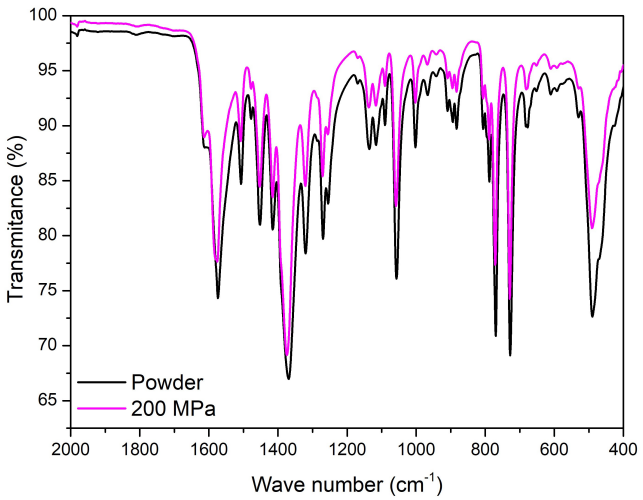

Figure 7. FTIR spectra of STAM-17-OET in both powder form (black) and 200 MPa tablet (magenta).

accessibility and diffusion of N_2 through the framework ultramicropores may have been limited to some extent. At non-cryogenic conditions, slightly smaller molecule of CO_2 compared to N_2 can overcome activation barriers for diffusion through very narrow openings, thus enabling their evaluation more accurately.[32] Indeed, the BET surface areas extracted from CO_2 isotherms obtained at 273 K (Figure 8) for the investigated materials show significantly higher values varying from 126 to 143 m^2/g indicating better accessibility of CO_2 molecules if compared to the N_2 ones. Moreover, the compression apparently does not have any effect on CO_2 diffusion, since no correlation between the applied pressure and BET values can be drawn. This result proves that the micropores retain their properties and then the porosity of STAM-17-OEt can be considered basically unaffected by the applied pressure.

The micropore accessibility for CO_2 molecules offers also additional information about the specific chemical properties of the densified materials. Due to the quadrupolar nature of the CO_2 molecule, its adsorption affinity (i.e. isosteric heat of adsorption) can be affected by the presence of polar sites (see Figure S13). Such polar sites can arise from structure defects

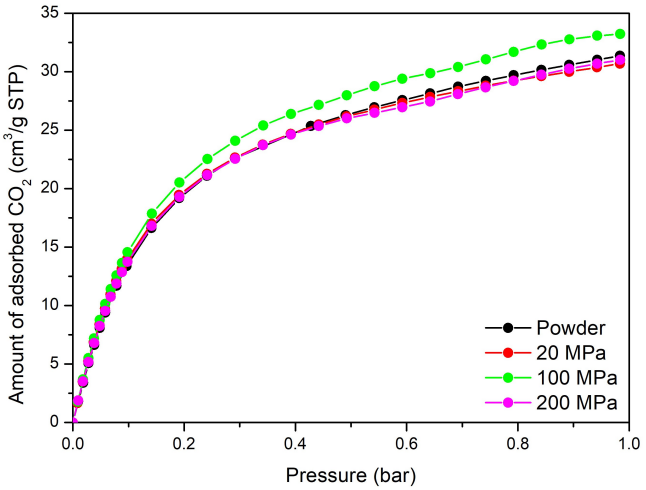

Figure 8. CO_2 isotherms acquired for the selected tablets of the set A measured at 273 K. The isotherm obtained for the powdered material is shown in black for comparison.

generated by the compression of STAM-17-OEt framework; indeed, the heat of adsorption at zero coverage gradually increases with the applied pressure from −16.2 to −27.6 kJ/mol. Even though the accessibility for CO_2 molecules remains more or less unchanged, the pressurization apparently promotes the tendency of CO_2 to bind to the framework. The defects that can create coordinatively unsaturated Cu(II) sites can be evaluated by Lewis acidity of the investigated materials. For this reason, both powdered STAM-17-OEt and the correspondent 200 MPa tablet have undergone catalytic cycloaddition reaction of propylene oxide to propylenecarbonate in presence of CO_2 at T = 373 K and pressure of 20 bar for 4 hours (see Figure S14). The powder sample product exhibits relatively low catalytic activity of propylene oxide (PO) to propylene carbonate (PC) conversion with the rate of 14% and selectivity of 87.6% resulting in the total PC yield of 12.4%. In contrast, the use of the tablet (200 MPa) significantly increases the conversion rate to 24% and, even though the selectivity is somewhat hindered compared to the powdered material, the total PC yield improves to 18.1%. The enhanced catalytic activity of the STAM-17-OEt structure after compression can be related to the increased Lewis acidity, which may originate from the defect formation, as already suggested by the CO_2 sorption enthalpy study.

Conclusions

The present study proves that STAM-17-OEt is a MOF able to withstand high pressures without significant damages, without loosing its granular form, maintaining its crystallinity, its peculiar flexibility and hemilability and the strong chemical stability with respect to water. Furthermore, through the study of CO_2 isotherms, we found that even the microporosity resulted unchanged upon compaction. Another very significant result is that, in contrast to what typically found for many framework compounds, not only did the compacted material show the persistence of catalytic sites after the application of a large pressure, but also the catalytic activity increased compared to that of the pristine STAM-17-OEt powder. The high resistance of the material towards the mechanical pressures applied allows the preparation of tablets of STAM-17-OEt which preserve the properties of the pristine materials and, at the same time, gives the advantages of a sample very well packaged in space, with a value of the effective density comparable with that of the bulk crystal. Our conclusions are fully supported by the results we have obtained with all the techniques used.

Our results are very significant from more than one point of view. Firstly, we have highlighted that STAM-17-OEt is a MOF which can be already considered ready for its industrialization: in fact, it has brilliantly overcome both the obstacles of water instability and of low packaging, which, in contrast, still affect the majority of MOF. Secondly, this aspect opens the doors for lots of new perspectives concerning this new MOF, since its performances can now be tested with the further advantage of a high packing density, generally rare for this category of MOFs simply synthesized as standard powders.[5] Then, regarding the limited amount of defects generated upon the application of the pressure and suggested by the XRD patterns, the EPR spectra and the CO_2 isotherms, not only do the defects not compromise the crystallinity or the structural properties of the material, but they can even increase the catalytic activity, as obtained in our experiment. Lastly, although STAM-17-OEt is not yet known enough to be considered a benchmark MOF, the combination of such outstanding properties in a single densified structure (mechanical and water stability, flexibility, hemilability, catalytic activity, preserved microporosity,…) sets new high levels of potentialities for the ever-increasing family of MOFs.

Experimental Section

STAM-17-OEt was synthetized as described by McHugh et al.[7] The activation was done by heating at T = 420 K in vacuum overnight. The dehydrated samples thus obtained are termed simply "activated powder". A set of tablets (named set A) have been produced from about 150 mg of activated powder, placed inside a pill maker under a hydraulic press and pressed for 10 minutes by applying a specific mechanical pressure. A set of samples was obtained, by using the following values of pressure: 3, 20, 50, 100, 150 or 200 MPa. In the following, all these samples will be referred to as "tablets". After preparation, each tablet was crushed and reactivated at T = 420 K overnight. The rehydration has been done by exposure to air moisture for about 2 hours keeping the powder in an open vial. Another set of tablets has been produced (named set B), with the only difference that the starting powder samples have been previously kept exposed to air moisture for about 20 minutes on a petri dish.

EPR measurements were performed using a Bruker EMX micro spectrometer working at a frequency of about 9.5 GHz (X-band) at temperatures of 77 and 300 K. The spectra were acquired using a dewar flask containing the EPR glass tube with the sample. Only for measurements at 77 K, the dewar flask was filled with liquid

nitrogen. All the spectra reported below were normalized for experimental parameters and for the mass of the samples.

Powder X-ray diffraction (PXRD) Diffraction patterns were collected using a PANalytical Empyrean with Cu X-ray tube and primary beam monochromator (CuKα1). Measurements are performed at 300 K.

Raman measurements have been acquired in the region from 150 to 1750 cm^{-1} with Bruker Senterra μ-Raman spectrometer equipped with a laser diode working at $\lambda = 532$ nm, with resolution of 9–15 cm^{-1} and the power of the laser set at 0.2 mW. During the measurements the samples were kept in air on a laboratory slide. The optical images have been acquired using the microscope of the μ-Raman spectrometer.

Fourier Transform Infrared (FTIR) spectra were recorded on a PerkinElmer Spectrum Two FT-IR spectrometer.

AFM measurements were done in air by a Bruker FASTSCAN microscope working in a soft tapping mode and using a FAST-SCAN-A probe (27 μm long triangular silicon nitride cantilever) with the following characteristics: 1500 kHz resonant frequency, 17 N/m force constant and about 5 nm apical radius. The size of the AFM images were 3 μm × 3 μm or 3 μm × 1.5 μm, depending on the local surface properties.

Nitrogen isotherms have been acquired by a Quantachrome IQ3 sorption analyser. Samples were degassed at 420 K for 16 hours prior the measurements.

CO_2 sorption measurements were performed on IMI-HTP gas analyser (Hiden Isochema Inc.) at different temperatures up to 1 bar. For the purposes of BET surface area calculations, the isotherm measured at 273 K was used, whereas the isosteric heat of adsorption determination was based on Clausius-Clayperon calculations from the isotherms taken at 298 and 303 K.

The catalytic activity of activated powder and the tablet pressed at 200 MPa were tested using the reaction of propylene oxide (PO) and CO_2 to produce propylene carbonate (PC) with the use of tetrabutylammonium bromide (TBABr) as co-catalyst. Before the reaction, the selected catalyst was degassed under the vacuum at 423 K for 16 h. For the reaction, 20 ml of PO, 0.1 g of TBAB and 0.10 g of activated powder or tablet were added to a 100 ml stainless steel high-pressure reactor (Parr). When the reaction mixture reached 383 K, the reactor was pressurized to 20 bar with CO_2 (99.99999 %). During cycloaddition, the reaction vessel was connected to the CO_2 source via a one-way check valve to maintain the pressure in the reactor. After four hours of reaction time, the reactor was rapidly cooled in an ice bath and the pressure was slowly released by opening the outlet valve. The catalyst was separated by filtration. Liquid state NMR spectroscopy was used to determine the rates of propylene carbonate formation. For the measurement 25 μl of the reaction mixture was dissolved in 500 μl DMSO-d6 and transferred into 5 mm NMR tubes. ^{1}H NMR spectra were recorded at 298 K on a Bruker Avance Neo 600 MHz NMR spectrometer with a BB(F)O SmartProbe. 16 scans were acquired for each spectrum, with a 30 s relaxation delay, 30° pulse and 65536 points. Conversion rates were determined based on integrals of the methyl group signals.

Supporting Information

Additional EPR measurements; Raman and FTIR spectra acquired for powder and tablets; AFM images acquired for a tablet 100 MPa and a sample of powder of STAM-17-OEt, accompanied by optical images; the estimated and calculated values of density for each sample studied; nitrogen isotherms and corresponding BET surface areas estimated; surface areas calculated from the CO_2 isotherms; results of the catalysis experiment.

Acknowlegements

The authors would like to thank people of the LABAM group (http://www.unipa.it/lamp/) at the Department of Physics and Chemistry of University of Palermo for useful discussions and support. AFM measurements were performed at the Advanced Technologies Center (http://www.atencenter.com). Financial support by PJ-RIC-FFABR_2017 and the EPSRC grant EPSRC industrial CASE award (grant EP/N50936X/1) are acknowledged. The research programme Nanoporous materials (P1-0021) financially supported by Slovenian Research Agency (ARRS) is acknowledged as well. We thank Uroš Javornik (National Institute of Chemistry, Slovenia) for the measurements and analysis of liquid NMR spectra.

Conflict of Interest

The authors declare no conflict of interest.

Keywords: EPR spectroscopy · Flexible MOFs · Metal-organic frameworks · MOF stability · MOF tableting

[1] H. Furukawa, K. E. Cordova, M. O'Keeffe, O. M. Yaghi, *Science* **2013**, *341*, 1230444.
[2] A. Schneemann, V. Bon, I. Schwedler, I. Senkovska, S. Kaskel, R. A. Fischer, *Chem. Soc. Rev.* **2014**, *43*, 6062–6096.
[3] N. C. Burtch, H. Jasuja, K. S. Walton, *Chem. Rev.* **2014**, *114*, 10575–10612.
[4] M. I. Nandasiri, S. R. Jambovane, B. P. McGrail, H. T. Schaef, S. K. Nune, *Coord. Chem. Rev.* **2016**, *311*, 38–52.
[5] T. Tian, Z. Zeng, D. Vulpe, M. E. Casco, G. Divitini, P. A. Midgley, J. Silvestre-Albero, J.-C. Tan, P. Z. Moghadam, D. Fairen-Jimenez, *Nat. Mater.* **2018**, *17*, 174–179.
[6] B. B. Shah, T. Kundu, D. Zhao, *Metal-Organic Framework* **2020**, 339–372.
[7] L. N. McHugh, M. J. McPherson, L. J. McCormick, S. A. Morris, P. S. Wheatley, S. J. Teat, D. McKay, D. M. Dawson, C. E. Sansome, S. E. Ashbrook, et al., *Nat. Chem.* **2018**, *10*, 1096.
[8] A. Terracina, L. N. McHugh, M. Todaro, S. Agnello, P. S. Wheatley, F. M. Gelardi, R. E. Morris, G. Buscarino, *J. Phys. Chem. C* **2019**, *123*, 28219–28232.
[9] D. M. Dawson, C. E. Sansome, L. N. McHugh, M. J. McPherson, L. J. M. McPherson, R. E. Morris, S. E. Ashbrook, *Solid State Nucl. Magn. Reson.* **2019**, *101*, 44–50.
[10] L. N. McHugh, A. Terracina, P. S. Wheatley, G. Buscarino, M. W. Smith, R. E. Morris, *Angew. Chem. Int. Ed.* **2019**.
[11] J. Kim, S.-H. Kim, S.-T. Yang, W.-S. Ahn, *Microporous Mesoporous Mater.* **2012**, *161*, 48–55.
[12] G. W. Peterson, J. B. DeCoste, T. G. Glover, Y. Huang, H. Jasuja, K. S. Walton, *Microporous Mesoporous Mater.* **2013**, *179*, 48–53.
[13] J. Dhainaut, C. Avci-Camur, J. Troyano, A. Legrand, J. Canivet, I. Imaz, D. Maspoch, H. Reinsch, D. Farrusseng, *CrystEngComm* **2017**, *19*, 4211–4218.
[14] J. Purewal, D. Liu, J. Yang, A. Sudik, D. Siegel, S. Maurer, U. Müller, *Int. J. Hydrogen Energy* **2012**, *37*, 2723–2727.
[15] D. Bazer-Bachi, L. Assié, V. Lecocq, B. Harbuzaru, V. Falk, *Powder Technol.* **2014**, *255*, 52–59.
[16] Y. H. Hu, L. Zhang, *Phys. Rev. B* **2010**, *81*, 174103.

[17] G. W. Peterson, J. B. DeCoste, F. Fatollahi-Fard, D. K. Britt, *Ind. Eng. Chem. Res.* **2014**, *53*, 701–707.
[18] J. Ren, T. Segakweng, H. W. Langmi, B. C. North, M. Mathe, *J. Alloys Compd.* **2015**, *645*, S170–S173.
[19] W. Y. Hong, S. P. Perera, A. D. Burrows, *Microporous Mesoporous Mater.* **2015**, *214*, 149–155.
[20] A. H. Valekar, K.-H. Cho, U.-H. Lee, J. S. Lee, J. W. Yoon, Y. K. Hwang, S. G. Lee, S. J. Cho, J.-S. Chang, *RSC Adv.* **2017**, *7*, 55767–55777.
[21] I. Majchrzak-Kucęba, A. Ściubidło, *J. Therm. Anal. Calorim.* **2019**, *138*, 4139–4144.
[22] A. Terracina, M. Todaro, M. Mazaj, S. Agnello, F. M. Gelardi, G. Buscarino, *J. Phys. Chem. C* **2018**, *123*, 1730–1741.
[23] M. Todaro, G. Buscarino, L. Sciortino, A. Alessi, F. Messina, M. Taddei, M. Ranocchiari, M. Cannas, F. M. Gelardi, *J. Phys. Chem. C* **2016**, *120*, 12879–12889.
[24] M. Todaro, A. Alessi, L. Sciortino, S. Agnello, M. Cannas, F. M. Gelardi, G. Buscarino, *J. Spectrosc.* **2016**, *2016*.
[25] M. Todaro, L. Sciortino, F. M. Gelardi, G. Buscarino, *J. Phys. Chem. C* **2017**, *121*, 24853–24860.
[26] S. S.-Y. Chui, S. M.-F. Lo, J. P. Charmant, A. G. Orpen, I. D. Williams, *Science* **1999**, *283*, 1148–1150.
[27] A. Pöppl, S. Kunz, D. Himsl, M. Hartmann, *J. Phys. Chem. C* **2008**, *112*, 2678–2684.
[28] X. X. Zhang, S. S.-Y. Chui, I. D. Williams, *J. Appl. Phys.* **2000**, *87*, 6007–6009.
[29] A. Rodríguez-Fortea, P. Alemany, S. Alvarez, E. Ruiz, *Chem. Eur. J.* **2001**, *7*, 627–637.
[30] E. Borfecchia, S. Maurelli, D. Gianolio, E. Groppo, M. Chiesa, F. Bonino, C. Lamberti, *J. Phys. Chem. C* **2012**, *116*, 19839–19850.
[31] Z. Chang, D.-H. Yang, J. Xu, T.-L. Hu, X.-H. Bu, *Adv. Mater.* **2015**, *27*, 5432–5441.
[32] K. C. Kim, T.-U. Yoon, Y.-S. Bae, *Microporous Mesoporous Mater.* **2016**, *224*, 294–301.

Manuscript received: February 15, 2021
Revised manuscript received: May 14, 2021
Accepted manuscript online: May 18, 2021